RESEARCH ARTICLE | JUNE 11 2025

Microcavity-based parallel measurements of optical power and wavelength

Yan Wang ; Yu-Hao Hu ; Jin-Lei Wu ; Jian Tang; Ya-Feng Jiao ; Ya-Chuan Liang; Hai-Yan Wang; Li-Ying Jiang ; Le-Man Kuang ; Ke-Yu Xia ; Lei Shi ; Hui Jing

Appl. Phys. Rev. 12, 021421 (2025)
https://doi.org/10.1063/5.0268412

Applied Physics Reviews ARTICLE pubs.aip.org/aip/are

Microcavity-based parallel measurements of optical power and wavelength

Cite as: Appl. Phys. Rev. **12**, 021421 (2025); doi: 10.1063/5.0268412
Submitted: 1 March 2025 · Accepted: 27 May 2025 ·
Published Online: 11 June 2025

Yan Wang,[1,a] Yu-Hao Hu,[1] Jin-Lei Wu,[2] Jian Tang,[3] Ya-Feng Jiao,[1] Ya-Chuan Liang,[1] Hai-Yan Wang,[1] Li-Ying Jiang,[1] Le-Man Kuang,[1,3] Ke-Yu Xia,[4,b)] Lei Shi,[5,6,b)] and Hui Jing[1,3,b)]

AFFILIATIONS

[1]School of Electronics and Information, Academy for Quantum Science and Technology, Zhengzhou University of Light Industry, Zhengzhou 450001, China
[2]School of Physics and Microelectronics, Zhengzhou University, Zhengzhou 450001, China
[3]Key Laboratory of Low-Dimensional Quantum Structures and Quantum Control of Ministry of Education, Department of Physics and Synergetic Innovation Center for Quantum Effects and Applications, Hunan Normal University, Changsha 410081, China
[4]College of Engineering and Applied Sciences, National Laboratory of Solid State Microstructures, Nanjing University, Nanjing 210023, China
[5]Wuhan National Laboratory for Optoelectronics, Huazhong University of Science and Technology, Wuhan 430074, China
[6]Optics Valley Laboratory, Wuhan 430074, China

[a)]**Electronic mail**: ywang@zzuli.edu.cn
[b)]**Authors to whom correspondence should be addressed:** keyu.xia@nju.edu.cn; lshi@hust.edu.cn; and jinghui@hunnu.edu.cn

ABSTRACT

Accurate determination of light power and wavelength is fundamental to nearly all optical and laser applications. However, simultaneous and precise measurements of these two parameters remain a critical challenge due to intrinsic cross-sensitivity in conventional devices. Here, we propose and demonstrate a dual-parameter decoupling strategy based on photothermal whispering gallery mode (WGM) microcavities, enabling parallel measurements of both optical power and wavelength without cross-sensitivity. Optical absorption of the pump light by the composite microcavity produces increased temperatures that are proportional to the pump power and wavelength of the light, resulting in a wavelength shift in the WGM resonance of the microcavity. We demonstrate a record-high photothermal tuning sensitivity of ~ -4 nm/mW and an ultralow detection limit of thermal power down to 4 μW, both of which surpass all previous schemes by more than an order of magnitude. With a linear response to the pump wavelength, the designed microcavity allows for near-infrared wavelength measurement over a broad bandwidth from 780 to 1064 nm. Importantly, by introducing the decoupling strategy that employs spectral changes of two microcavities with asymmetric responses, we demonstrate parallel measurements of both optical power and wavelength with high accuracy. As the first proof-of-principle demonstration of a single optical power–wavelength measurer using optical microcavities, our work could advance various applications relying on miniaturized and precise optical metrology devices.

I. INTRODUCTION

Optical power and wavelength are crucial parameters in optical signal analysis and measurement. Accurate determination of these two parameters is fundamental to applications in fiber optic communication,[1] optical sensing,[2] and laser processing,[3] ensuring precision and consistency of data transmission and device production. In scientific research and analysis, simultaneous measurements of optical power and wavelength are of particular significance in terms of improving measuring efficiency and accuracy, as well as revealing transient processes and physical mechanisms of light–matter interaction. Moreover, it plays an especially crucial role in the emergent quantum research, where concurrent and precise control of the laser power and wavelength is essential for experiments associated with quantum information, computing, and sensing.[4–6] However, simultaneous and precise determination of optical power and wavelength persists as a significant challenge in optical and photonic metrologies, as conventional approaches are constrained by the tradeoffs between performance, complexity and functionality. Consequently, separate devices, such as optical power meters and wavemeters, are used to measure one of the two. The optical power meters can operate with high accuracy only

when the wavelength of the source being tested is known, and a slight wavelength deviation could lead to an acute power reading error, that is the so-called cross-sensitivity. For the wavemeters, although state-of-the-art techniques relying on speckle patterns and frequency combs can offer ~femtometer resolution[7–9] and kilohertz-level precision,[10–12] these approaches necessitate complex calibration protocols, such as transmission matrix reconstruction and dual-laser stabilization, and in particular, lack the ability to accurately measure optical power. Moreover, the accuracy of the wavemeters is generally affected by the laser power, manifesting as significantly degraded accuracy at low and high powers. Even integrated spectrometers leveraging disordered scattering media, metasurfaces, and programmable photonic circuits prioritize spectral analysis rather than absolute power quantification,[13–16] also demanding periodic and complex calibration. The limitations in all these existing techniques stem from a pervasive optimization paradigm of a single parameter in optical sensing, where the advances in the measurement performance and miniaturization come at the expense of functional versatility.

Optical whispering-gallery-mode (WGM) microcavities have advanced the developments in fundamental science and technology in the past decades, including optomechanics,[17–20] non-Hermitian physics,[21] frequency combs,[22] imaging,[23] lasers,[24–27] and sensors.[28–31] The WGM microcavities,[32] which confine resonant photons in a highly confined volume for a long period of time, strongly enhance the interaction of light with analytes, leading to ultrasensitive sensing.[33,34] The microcavity-based sensors generally exploit the changes in their spectral characteristics induced by the signal of interest, such as broadening,[35] splitting,[28,29] and wavelength shift[36–38] of the resonant modes. Photothermal regulation of the mode shift is highly attractive due to its distinctive merits of high tuning speed and large tuning range,[39,40] and in particular, the great potential in developing all-optical tunable photonic devices.[41] In addition, simultaneous measurement of multiple parameters has recently become the subject of growing interest in the field due to the quest for acquiring multi-dimensional information in practical scenarios. A self-referencing strategy employing two selected cavity modes has been proposed to precisely decouple different physical quantities.[42,43] However, the potential of microcavity-based strategies with optical signal decoupling capability remains to be sufficiently explored.

In this work, we address the aforementioned challenge by proposing a novel dual-WGM-microcavity architecture that enables decoupled optical power–wavelength measurement, for the first time achieving high-precision parallel metrology within a single compact device. The architecture leverages a composite microcavity fabricated through the integration of magnetic nanoparticles (MNPs) into a polymer-coated silica microsphere. The incorporation of MNPs imparts spectrally broadband photothermal responsiveness to the microcavity, facilitating all-optical tuning of the WGM resonance. With the formation of the WGM resonance in the polymer coating, the composite microcavity features a high quality (Q) factor in excess of 10^8, which is used as a sensitive detector for pump power measurement. We demonstrate a photothermal sensitivity of ~ -4 nm/mW and a detection limit of thermal power down to 4 μW. Compared to all previous works based on photothermal microcavities,[39,40,44–52] our implementation achieves more than an order of magnitude improvement in both sensitivity and detection limit. Remarkably, we highlight the response of the photothermal microcavity to the pump wavelength, which was neglected in previous works.[39,40,44–52] We demonstrate that the microcavity can exhibit linear and broadband spectral responses to the pump wavelength, enabling near-infrared (NIR) wavelength measurement ranging from 780 to 1064 nm. Remarkably, by developing a decoupling strategy that employs spectral changes of two microcavities with asymmetric responses, we realize parallel measurements of the laser power and wavelength with high accuracy. Our technique opens up new avenues toward miniaturized and precise optical metrologies, and holds great potential for a broad range of applications, such as the actively developing quantum technologies requiring simultaneous laser power and wavelength quantification[53,54] and industrial laser processing demanding real-time monitoring.[55,56]

II. RESULTS AND DISCUSSION

A. Microcavity fabrication and characterization

The developed microcavity is composed of a MNP-doped silica microsphere and a polymer coating, and its fabrication procedures are shown in Fig. 1(a). A fiber tip with a diameter of approximately 10 μm was first fabricated by heating and pulling a single-mode fiber with an oxyhydrogen (OH) flame [steps (i) and (ii), see Sec. IV A for details]. The tapered region was subsequently coated with MNPs through deposition of the mixed MNP solution [step (iii)]. Upon CO_2 laser ablation, a silica microsphere containing internally doped MNPs with uniform surface morphology was formed [step (iv)]. The microsphere then underwent repeated immersion in poly(methylmethacrylate) (PMMA) solution for polymer coating [step (v) and inset]. The spectral characterization of the microsphere cavity was performed using the experimental setup schematically illustrated in Fig. 1(b). The microcavity was probed by either a broadband light source or a tunable laser via tapered-fiber coupling (see Sec. SIV and Fig. S1 in the supplementary material), and the transmission spectrum of the microcavity was monitored in real time. NIR pump lasers (with wavelengths in the linear absorption range of MNPs) were chosen as heat sources, which were axially injected into the microcavity through the fiber stem to trigger the photothermal effect. Decoupling the pump and probe in our two-beam configuration facilitates easy regulation of pump power without affecting probe beam coupling. Note here that the power of the probe light was kept at a low level to avoid interference from thermal effects. In addition, the WGM resonances can be well confined within the polymer coating of the microcavity (see numerical demonstrations below), implying that the probe light at the resonant wavelengths can hardly be injected downward along the fiber stem. Even if any probe light at the non-resonant wavelengths entering the silica microsphere is absorbed by the MNPs, the resulting photothermal heating of the microsphere and the subsequent effect on the resonance of microcavity would be negligible due to the extremely low probe power. The microcavity–fiber coupling [top left inset in Fig. 1(b)] was monitored under an imaging system. The device was placed inside a home-built chamber to minimize the interference from air flow and contaminants.

Figure 1(c) shows the transmission spectrum of an 81-μm-diameter microsphere cavity (featuring a 75-μm-diameter silica core and a 3-μm-thick PMMA shell), where typical WGM resonant modes are revealed. The free spectral range (FSR), determined by the spectral range between the lowest radial modes, is found to be 6.54 nm. Theoretically, the FSR in a circular WGM resonator can be expressed by FSR $\sim \lambda^2/\pi n_{\mathrm{eff}} D$, where λ, n_{eff} and D are the central wavelength of the resonance spectrum, effective refractive index and diameter of the microcavity, respectively. The theoretical FSR is calculated to be 6.53 nm, which is very close to the experimentally measured value.

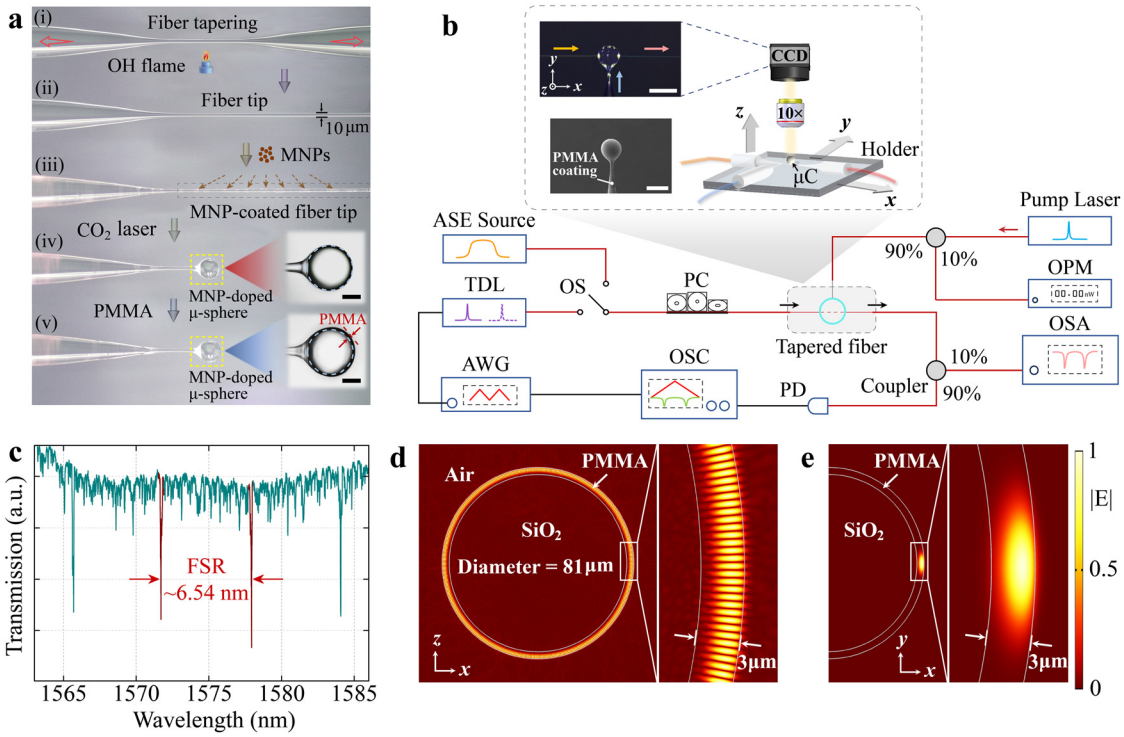

FIG. 1. Fabrication and spectral characterization of the microcavity. (a) Micrographs showing the fabrication procedures of the polymer-coated microsphere (μ-sphere) cavity doped with MNPs. Scale bars: 30 μm. (b) Schematic of the experimental setup for characterizing and implementing photothermal tuning of the microsphere cavity. The top box illustrates the imaging system for monitoring in real time the microcavity (μC) coupled to the tapered fiber, and the left insets show, respectively, the dark-field micrograph and the SEM image of the microcavity. Scale bars: 100 μm. TDL: tunable diode laser; OS: optical switch; PC: polarization controller; OPM: optical power meter; OSA: optical spectrum analyzer; AWG: arbitrary waveform generator; PD, photoelectric detector; OSC: oscilloscope. (c) Transmission spectrum of an 81-μm-diameter microsphere cavity (with a 75-μm-diameter silica core and a 3-μm PMMA shell), with FSR of 6.54 nm. (d) and (e) Numerical simulations showing electric field |E| distributions on the x–z and x–y planes of the microsphere cavity with the same size as in (c).

For the proposed polymer-coated microsphere cavity, the WGM fields are well confined within the PMMA layer due to a higher refractive index ($n_{\text{eff}} = 1.49$) than the silica core ($n_{\text{sil}} = 1.45$). This is further verified by numerically simulating the electric field distribution in the microcavity (see details in Sec. SII of the supplementary material). Figures 1(d) and 1(e) show the cross-sectional views of the electric field distributions inside the microcavity. As expected, the light fields are almost entirely confined in the PMMA layer, with only a few (about 6%) leaking into the adjacent domain (Fig. S2, supplementary material). This implies that the probe light at the resonant wavelengths can hardly be injected downwards along the fiber stem. Such an efficient confinement of light contributes to the formation of high-Q WGM resonance. Moreover, the PMMA-coated microcavity has an extremely smooth surface and a nearly perfect circular boundary [see the SEM image in Fig. 1(b)], which also facilitates the improvement of the Q factor.

The Q factor of the microcavity was characterized based on the experimental setup shown in Fig. 1(b). Four types of microcavities with different structures [insets in Fig. 2(a)] were prepared for Q-factor measurement. In experiments, resonance modes with the highest Q factors were extracted separately from the transmission of ten microcavities of each type (Sec. SIII, supplementary material). The results of the measured Q factors are summarized in Fig. 2(a). The raw silica microspheres exhibit a mean Q factor exceeding 2.6×10^8, with typical transmission spectra being illustrated in Fig. 2(b). A representative ringing phenomenon in the tail of the transmission is observed, revealing an ultrahigh Q factor of 2.69×10^8 (corresponding to a cavity photon lifetime of about 450 ns). The limitation of such a Q factor includes the scattering due to the surface roughness and the absorption in the silica. In comparison, the silica microspheres after the PMMA coating exhibit reduced Q factors [Fig. 2(c)] with a mean value of 1.2×10^8, which is due to a higher absorption loss of the PMMA. This means that the additional coating cannot lead to a significant decrease in the Q factor, confirming geometrical perfection of the coating. In contrast, the Q factors of the microspheres after doping MNPs (with a concentration of 5 wt. %) are significantly degraded to the level of 10^4 [Fig. 2(d)], which is caused by the extremely strong absorption from the MNPs. Further increasing the concentration of the doped MNPs leads to a further deterioration of the Q factor (Fig. S4, supplementary material). By coating these low-Q microcavities with a PMMA layer, their WGM fields can be well isolated from the internally doped MNPs [Figs. 1(d) and 1(e)], keeping the MNPs away from the mode volume of WGMs. With remarkably reduced absorption loss, ultrahigh Q factors exceeding 10^8 are observed as expected [Fig. 2(e)], which is comparable to those without MNP doping [Fig. 2(c)]. Note that such a high Q factor is within reach even for a higher doping concentration

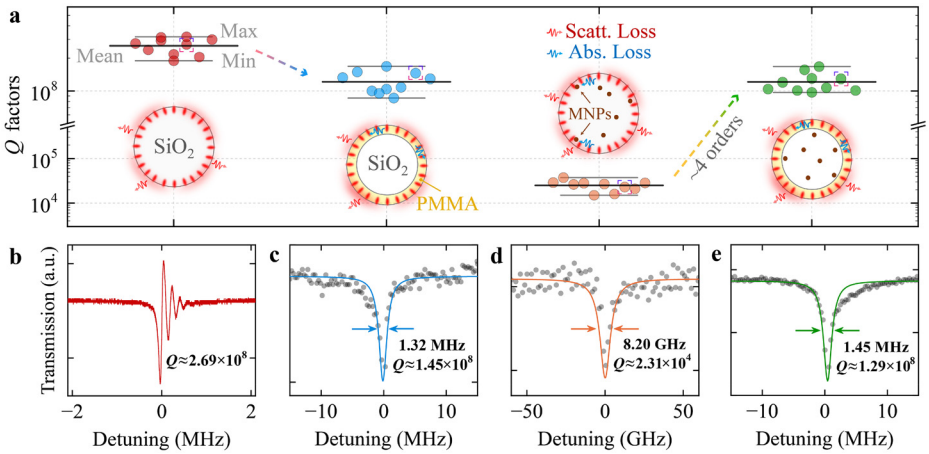

FIG. 2. *Q*-factor characterization of the fabricated microsphere cavities. (a) Measured *Q* factors of four types of microcavities with different structures (insets), which are extracted separately from the highest-*Q* resonance modes of ten microcavities of each type. (b)–(e) Close-up of the transmission spectra showing typical *Q* factors of the four types of microcavities, orderly identified by the dashed boxes in (a). The diameters of all uncoated and coated microcavities used here are 75 and 81 μm, respectively. The curves are Lorentzian fitting to the experimental data.

(for example, 20 wt. %) of MNPs (Fig. S4, supplementary material). This reveals an extraordinary capability of the proposed polymer-coated microcavity in conserving high *Q* factor. As the *Q* factor relevant to the accumulation of light (i.e., optical field intensity) within the microcavity is crucial to the sensing performance, the proposed microcavity enables enhanced sensitivity in the photothermal tuning (as discussed below). It is noted that the evanescent field intensity in proximity to microcavity surfaces also plays a crucial role for optimizing sensing capabilities. Experimental evidence demonstrates that coating silica microspheres with a high-refractive-index polymer layer of subwavelength thickness can substantially enhance sensing sensitivity.[57]

B. All-optical photothermal tunability

Next, we demonstrate the feasibility of constructing all-optical tunable devices using the proposed microcavity. The basic idea is to transfer optical absorption of the microcavity to its resonance modulation via synergizing photothermal and thermo-optic effects. Specifically, a 980-nm pump laser as a heat source is axially injected into the microcavity and then absorbed by the MNPs to induce localized photothermal heating. Thermal energy transferred to the PMMA layer alters its refractive index via the thermo-optic effect, thereby modulating the WGM resonance wavelength. Real-time readout of resonance shift enables to derive optical excitation onto the microcavity. In experiments, the microcavity was kept in a thermostatic chamber to eliminate the influence of environmental thermal fluctuations. Figure 3(a) shows the absolute value of the wavelength shift $|\Delta\lambda|$ vs the pump power for the microcavities with different structures as demonstrated in Fig. 2. The MNP-doped microcavities (circles and squares) exhibit an evident shift in the resonant wavelengths (Sec. SIV, supplementary material). For the microcavities without MNPs (diamonds and hexagons), however, their responses to the pump laser are extremely weak, even when increasing the pump power to 100 mW. To quantify the capability of the spectral tuning, we introduce the photothermal tuning sensitivity, which is defined as the ratio of $\Delta\lambda$ to the pump power (unit: nm/mW). The experimental observation shows that the doped MNPs are indispensable for high tuning sensitivity. Moreover, the tuning sensitivity of the PMMA-coated microcavities is much higher than that of the uncoated microcavities. Among the four variants of microcavities, the composite microcavity (with both PMMA and MNPs) has the highest tuning sensitivity of approximately −4 nm/mW, which is at least an order of magnitude higher than that of the existing devices (see Sec. SV in the supplementary material for detailed comparison). As for the tuning range (i.e., the largest wavelength shift), a maximal value exceeding 13 nm is achieved for the MNP-doped microcavity without a coating under a pump power of 100 mW. This tuning range is comparable to that of the reported tunable microcavity devices (Table S1, supplementary material). In particular, a larger tuning range can be expected by further increasing the pump power. Note here that the composite microcavity was photothermally tuned within a narrow pump power range (less than 2 mW) to suppress thermal deformation-induced spectral fluctuations in the polymer coating. The power range could be extended by suitably decreasing the doping concentration of MNPs in the microcavities.

The unique property of the composite microcavity promises a high sensitivity and a low limit for measuring the pump power. To characterize this, we measured the wavelength shifts vs the pump power for three composite microcavities with different doping concentrations of MNPs. As shown in Fig. 3(b), the absolute values of the wavelength shifts increase monotonically with the pump power. Controlling the pump power within a small range (0–50 μW), an ultrahigh sensitivity up to approximately −13.5 nm/mW is achieved for the microcavity with the highest MNP concentration of 20 wt. %. Decreasing the doping concentration of MNPs leads to a lower light-to-heat conversion, resulting in the reduction in the tuning sensitivity. Despite this, a high sensitivity of approximately −3.6 nm/mW is still achievable for the microcavity with 5 wt. % MNPs. For a relatively small range of the pump power, the resonance of the composite microcavities can be tuned with a high linearity exceeding 0.99. As the pump power increases, the resonance shift gradually levels off, exhibiting a behavior akin to approaching steady state (due to the saturation of thermo-optic effect under high temperature). For practical measurement of the pump power, a linear response of the microcavity is highly desirable, which in turn requires linear tuning of the microcavity resonance. In our experiments, the linear tuning (i.e., power measurable) range was optimized by choosing suitable concentrations of the MNPs doped in the microcavities (see details below). In addition, the limit of detection is evaluated by further decreasing the pump power, followed by statistically analyzing the wavelength shifts. As shown in Fig. 3(c),

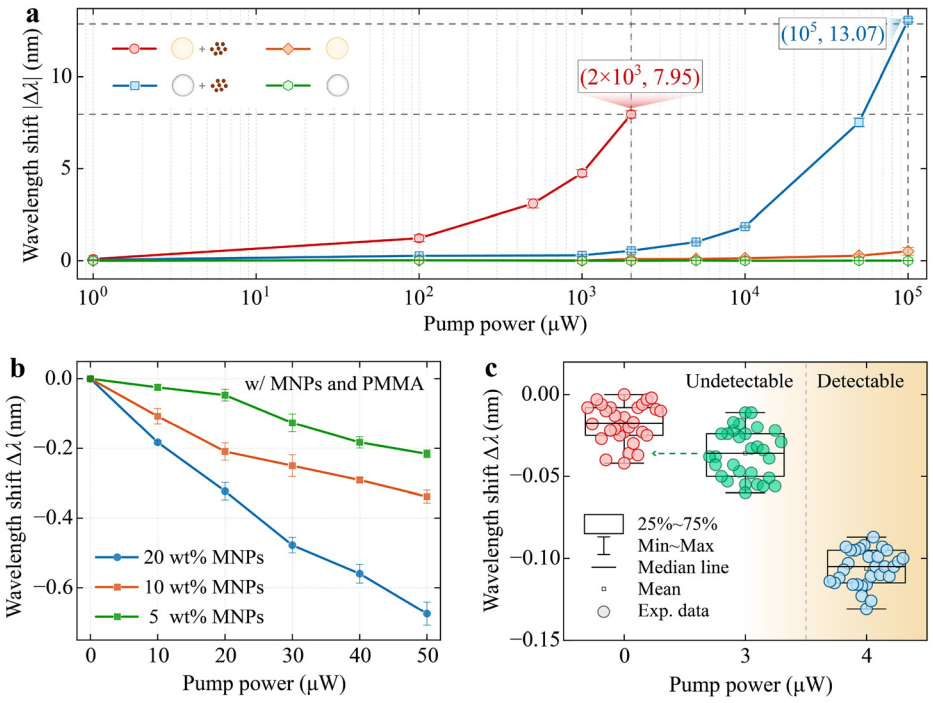

FIG. 3. All-optical tuning of WGM resonance for measurement of pump power. (a) Absolute value of the wavelength shift $|\Delta\lambda|$ vs the pump power for the microcavities with different structures as used in Fig. 2. (b) Wavelength shift $\Delta\lambda$ vs small-scale pump power for the composite microcavities with different doping concentrations of MNPs. (c) Statistical analysis of the wavelength shift $\Delta\lambda$ of the composite microcavity (with 20 wt. % MNPs) under pump powers of 0, 3, and 4 μW, showing a detection limit of 4 μW. The boxplots indicate confidence ranges of the experimental data (circles).

mean wavelength shifts of −36 and −105 pm are detected at the pump powers of 3 and 4 μW, extracted from the composite microcavity with 20 wt. % MNPs. For the pump power of 0 μW, a mean wavelength fluctuation of −17 pm is identified, which is a consequence of the thermal-refractive noise induced by the ASE source and the pump laser jitter. Notably, for the pump power of 3 μW, the wavelength shifts are mostly buried in the intrinsic wavelength fluctuations, which are too small to be resolved. When further increasing the pump power to 4 μW, distinguishable wavelength shifts are observed, unveiling the detection limit of the pump power. In comparison, for the composite microcavity with a lower MNP concentration of 10 wt. %, the detection limit increases to 10 μW (Sec. SVI, supplementary material).

C. Parallel measurement

The MNPs employed in the experiment can efficiently absorb light over visible, near-ultraviolet, and NIR bands. The energy of the absorbed light is then converted into heat, resulting in resonance shifts of the microcavity. The amount of conversion is generally characterized by the photothermal conversion efficiency (PCE) that reflects the percentage of absorbed photons converted into heat. It is known that the PCE is dependent on the wavelength of the pump light, which increases linearly in the NIR band (700–1300 nm) for the MNPs used in the experiment.[58] To explore the effect of the pump wavelength on the tuning performance, we measured the wavelength shift of the composite microcavity under several pump lasers of different wavelengths, with the pump power being fixed. One sees in Fig. 4(a) that for a certain pump power, the amplitude of the wavelength shift increases linearly with the pump wavelength, consistent with the trend of the PCE of MNPs. Also, for a larger pump power, the slope of the linear fitting line, defined as wavelength sensitivity, increases accordingly. This is reasonable because the PCE remains constant for a given pump wavelength. Therefore, proportional increase in the pump power inevitably leads to the wavelength shift increasing in the same trend. This can be seen more clearly by plotting the wavelength shift vs the pump power at different pump wavelengths (Sec. SVII, supplementary material). The linear dependence is of particular significance since it enables determination of the pump wavelength (within a certain range) by extracting the wavelength shift, thereby allowing for practical application to wavelength measurement. Moreover, acquiring the dependences of the resonance shift on the pump power [Figs. 3(a) and 3(b)] and the pump wavelength [Fig. 4(a)] provides pre-calibration procedures for practical measurements. It should be noted that although different fiber-stem geometries could induce distinct pre-calibration results, high-precision measurements remain achievable provided the dependences are acquired in advance.

The resolution of the wavelength measurement can be estimated via the wavelength sensitivity and the mode linewidth. The latter determines the smallest detectable resonance shift induced by the wavelength variation, which is typically 1/50 of the mode linewidth $\delta\lambda$.[30] For the fabricated high-Q microcavity, the measurable $\delta\lambda$ in current experiment is limited by spectral resolution of the OSA, which is considered as 0.02 nm. Taking the wavelength sensitivity of 6.7 pm/nm [extracted from the green line in Fig. 4(a)] as an example, the wavelength resolution is then deduced to be 0.06 nm. A lower wavelength resolution is expected by alternatively using a PD to enable high-resolution readout of the resonance shifts, which could be down to the level of tens of femtometers by assuming a modest mode linewidth of $\delta\lambda \sim 15$ fm ($Q \sim 10^8$). With optimized means of signal amplification and noise suppression,[36] further improvement of the performance could be feasible, promising a sub-femtometer-level resolution that is comparable to state-of-the-art speckle- and frequency comb-based wavemeters.[7,10]

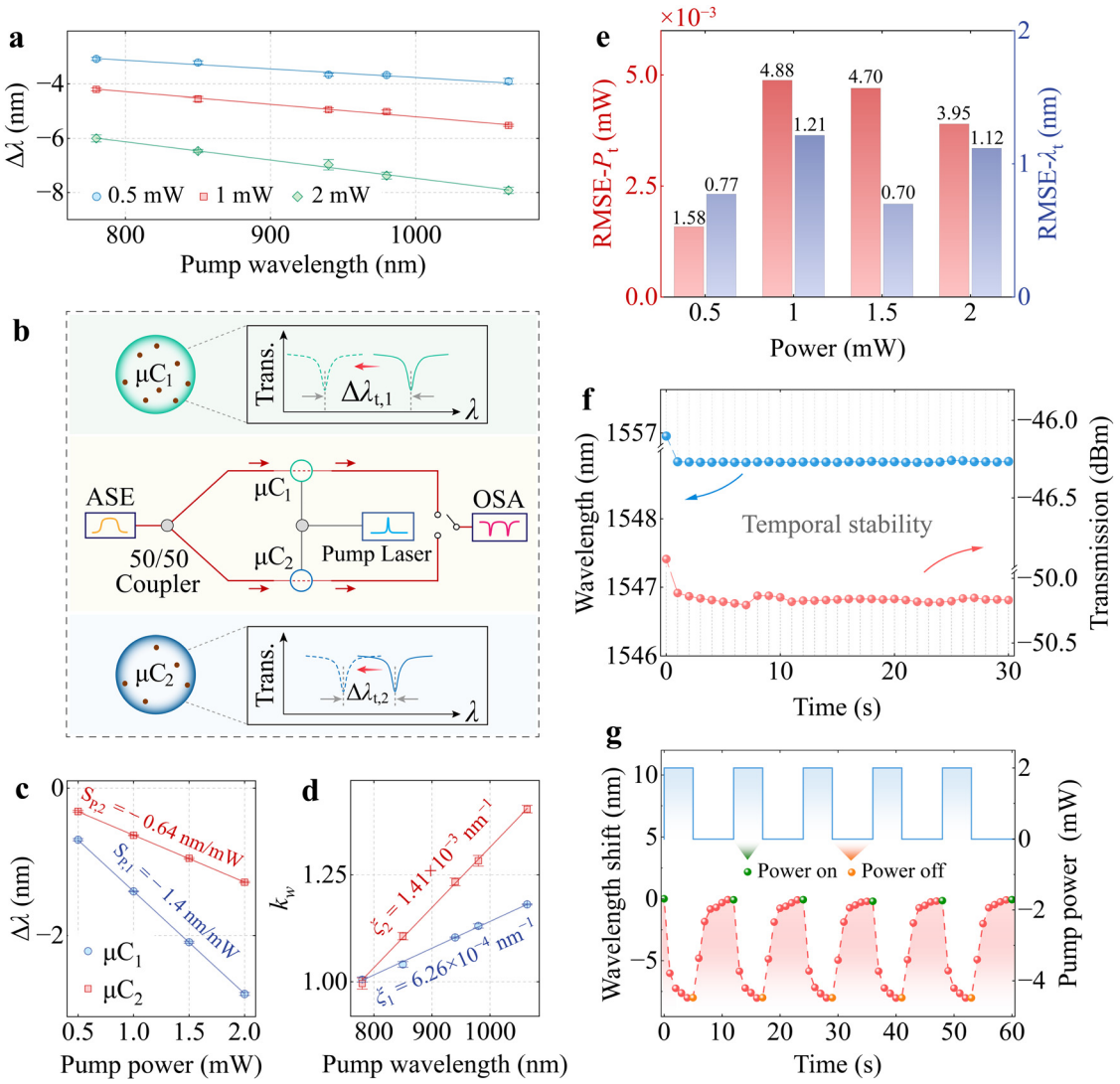

FIG. 4. Parallel measurements of optical power and wavelength. (a) Wavelength shift $\Delta\lambda$ vs five different pump wavelengths for the microcavity with 20 wt. % MNPs. The straight lines are linear fitting to the experimental data. (b) Schematic diagram of the experimental setup for parallel measurements of power and wavelength using a couple of microcavities. The probe light emitted from the ASE source is evenly divided into two beams that are coupled respectively to the two microcavities, and the transmission is recorded by an OSA. The pump laser to be measured is evenly divided and injected into the two microcavities through their fiber stems. (c) Power sensitivity S_{Pj} of two microcavity (doped, respectively, with 4 and 2 wt. % MNPs) under a 780 nm reference light. (d) Gain factor k_w vs pump wavelength. (e) RMSE of the measured power P_t and wavelength λ_t. The microcavities are pumped by an 830-nm laser with powers of 0.5, 1.0, 1.5, and 2.0 mW. (f) Wavelength shift of the microcavity vs five heating and cooling cycles. The green and yellow spheres mark the times at which the pump laser is turned on and off, respectively. Typical steady states during heating and cooling processes can be clearly identified. (g) Resonant wavelength and transmission intensity of the microcavity vs pump time. Despite continuous ongoing of the heating, the resonant wavelength can reach a steady state within seconds, which is a consequence of the thermal equilibrium established in the microcavity after a certain heating time.

Perhaps more interesting is the capability of the proposed composite microcavity for parallel optical power–wavelength measurement. Note that although these two parameters are involved in the spectral characteristics of a single microcavity as demonstrated above, it is still difficult to distinguish them from the spectra due to cross-sensitivity. We overcome this by engineering a dual-cavity configuration where spectral responses (i.e., power and wavelength sensitivities) of the two microcavities can be regulated on demand. With this strategy, the light to be measured induces different degrees of spectral variations in the two microcavities, based on which the power and wavelength of the light can be accurately decoupled. More details about the decoupling scheme are presented in Sec. SVII of the supplementary material. Experimentally extracting the wavelength shifts of the two microcavities allows for simultaneous readout of the unknown power and wavelength. The parameter equation established for dual-parameter decoupling has the form of (Sec. SVII, supplementary material)

$$S_{P,j}P_t[\xi_j(\lambda_t - \lambda_{in}) + 1] = \Delta\lambda_{t,j}, \quad (1)$$

where $S_{P,j}$ denotes the power sensitivity of the microcavity j ($j = 1, 2$) when subjected to a reference light with wavelength of $\lambda_{in} = 780$ nm, P_t and λ_t represent, respectively, the power and wavelength of the pump light to be measured, ξ_j is a given parameter that is introduced to correlate P_t and λ_t (Sec. SVII, supplementary material), and $\Delta\lambda_{t,j}$ is the experimentally measured wavelength shift of the microcavity j. In experiments, a dual-channel system was constructed to characterize the two microcavities, as schematically illustrated in Fig. 4(b). Alternatively, transmission spectra and resonance shifts of the two microcavities can also be recorded individually using two PDs to enable simultaneous measurement. The two microcavities were fabricated with low doping concentrations of MNPs, namely, 4% (μC_1) and 2% (μC_2), to ensure high linearities in their power sensitivities, which is important for high-precision measurement. Figure 4(c) shows the dependence of the wavelength shift of the two microcavities on the pump power when the pump wavelength is fixed to λ_{in}. The power sensitivities are $S_{P,1} = -1.4$ nm/mW and $S_{P,2} = -0.64$ nm/mW, respectively, with linearities both exceeding 99.99%. Figure 4(d) shows the gain factor k_w, defined by $k_w = \Delta\lambda_w/\Delta\lambda_{in}$ (with the subscript w denoting an arbitrary pump wavelength $\geq \lambda_{in}$), vs the pump wavelength, where $\xi_1 = 6.26 \times 10^{-4}\,\text{nm}^{-1}$ and $\xi_2 = 1.41 \times 10^{-3}\,\text{nm}^{-1}$ for the two microcavities can be derived (Sec. SVII, supplementary material). The feasibility of our scheme for parallel measurement is then explored by axially injecting a pump laser with a wavelength of 830 nm and different powers into the two microcavities [Fig. 4(b)]. Figure 4(e) shows the root mean square errors (RMSE) of the measured power and wavelength (Sec. SVIII, supplementary material), indicating reasonably good agreement with the true values. For practical applications, the reproducibility and stability of the microcavity are further examined, as shown in Figs. 4(f) and 4(g). The microcavity exhibits excellent reversibility and reproducibility, validated by unchanged wavelength shift in five cycles of consecutive heating–cooling–heating [Fig. 4(f)]. Furthermore, extremely small fluctuations of the resonant wavelength (<0.03 nm) and the extinction ratio (<0.1 dB) are observed in 30 min, demonstrating excellent temporal stability of the microcavity.

III. CONCLUSIONS AND OUTLOOK

In conclusion, we have developed photothermal WGM microcavities that facilitate unprecedented tuning performance and accomplished, for the first time, all-optical parallel measurements of optical power and wavelength. The developed composite microcavities feature ultrahigh Q factors up to 10^8, enabling a photothermal tuning sensitivity of ~ -4 nm/mW and a thermal power detection limit of 4 μW. The linear response of the microcavity to the laser wavelength was experimentally verified for broadband wavelength measurement. By engineering a dual-channel setup that employs two microcavities of different responses, parallel measurements of both optical power and wavelength were achieved with high accuracy. Furthermore, excellent reproducibility and stability of the microcavity were demonstrated, making it suitable for practical use. With these excellent functionalities, the developed technique not only eradicates the dependence of optical power measurement on accurate determination of wavelength but also surmounts the hurdles of insufficient precision and limited efficiency that are intrinsic to existing technologies.

The long-term reliability of microcavity-based devices in complex environments critically depends on stable packaging architectures. Existing encapsulation techniques, including wholly package, spot package, and holder package methods, provide critical insights for our future explorations to advance packaging designs of the developed device.[59–61] Our technique for high-performance parallel measurement is highly versatile and has broad compatibility. Through controllable adjustment of the concentrations and formulations of photothermal nanoparticles, both the detection range of optical power and the wavelength responsivity can be flexibly tuned, thereby enabling operation across broader spectra, e.g., extending to the visible and infrared regimes. Moreover, featuring μW-level detection capability of weak optical signal over a broad bandwidth, the developed dual-parameter-decoupling technique holds great potential for applications to diverse technological fields, particularly the rapidly emerging quantum technologies, advanced laser processing, and clinical therapeutics. Specifically, it opens up new opportunities for high-precision power–wavelength co-measurement, facilitating multiple functionalities including the control of single-photon source in quantum experiments,[53,62] dynamic calibration of integrated photonic chips,[54,63] and real-time monitoring of industrial laser processing.[55,56,64] Moreover, upon operating within the NIR wavelength band, our device addresses unique demands in photothermal therapy that require simultaneous laser power and wavelength quantification.[65,66] The inherent compatibility with standard NIR therapeutic wavelengths (e.g., 808 and 1064 nm) establishes the device as a compact and integrated platform for monitoring the therapeutic effects of laser-based tumor cell treatments, ensuring localized heating to therapeutic levels while minimizing the damage to surrounding healthy tissue.

IV. METHODS

A. Microcavity fabrication

The proposed microcavity is fabricated in a five-step process, as illustrated in Fig. 1(a). First, a single-mode fiber (SMF-28, Corning) with the coating being removed is fixed to two stepper motors. Then, an oxyhydrogen flame is used to heat the fiber while the stepper motors are electrically controlled to exert two opposite pulling force on the fiber, thereby forming a uniform tapered region [step (i)]. Upon controlling the stepping distance, a tapered region with a length of approximately 1 mm is finally achieved, characterizing a sharp tapered transition and a uniform elongated tapered waist [step (ii)]. For preparing the MNP-doped microcavity, iron oxide (II,III) nanoparticles (30 nm average particle size, purchased from Sigma-Aldrich), de-ionized water, and cyclohexane are first mixed with a weight ratio of 1:3:16, and the mixed solution with uniformly dispersed MNPs (5 wt. %) is then obtained after ultrasonically treating for 30 min. Subsequently, the mixed solution is dropped onto the tapered region of the fiber tip on which MNPs are uniformly distributed [step (iii)] after cyclohexane evaporates. Next, a carbon dioxide (CO_2) laser (Ti60, Synrad) beam is focused on the tapered region where MNPs are attached [Fig. S1(a), supplementary material]. Under the ablation of the CO_2 laser, a silica microsphere with a uniform surface and MNPs doped inside is formed [step (iv)] due to surface tension. Tuning the waist diameter and length of the tapered region allows precise control of the size of the MNP-doped microsphere; For example, a 75-μm-diameter microsphere is obtained for a waist diameter and taper length of about 10 μm and 1 mm, as shown in the insets in Fig. 1(a). Upon finely optimizing the parameters of the CO_2 laser, the fabricated microspheres exhibit excellent spherical morphology without apparent deformation. This implementation prevents the deterioration in the measurement accuracy caused by deformation-induced

mode splitting of the microcavity. In addition, for preparing the polymer coating of the microsphere cavity, poly(methylmethacrylate) (PMMA, Sigma-Aldrich) is first dissolved in tetrahydrofuran and then a PMMA solution is obtained after ultrasonic treatment for 2 h. The integrated fiber tip-microsphere structure provides a simple method for coating the PMMA onto the microsphere's surface, allowing us to flexibly submerge the microsphere into the polymer solution to complete uniform coating coverage [step (v)]. Also, it allows for triggering the photothermal effect of the doped MNPs by simply injecting the pump lasing through the fiber stem. The PMMA coating of different thickness can be deposited onto the microcavity by simply controlling the number of times of immersion in the polymer solution.

B. Experimental setup

A tapered fiber with a waist diameter of 2 μm is produced by heating and stretching the single-mode fiber using an oxyhydrogen flame, which is then fixed on a holder. A signal light emitted by an amplified spontaneous emission (ASE) light source (ASE-C+L-N, Hoyatek) is passed through a polarization controller (PC, FT-T56-PC, LBTEK) and transferred into the tapered fiber to excite the WGMs in the microcavity [Fig. S1(b), supplementary material]. A tunable diode laser (TDL, CTL1550, Toptica) is used for characterizing the Q factor of the microcavity, which is driven by a triangular wave signal from an arbitrary waveform generator (AWG, 33520B, Keysight) to perform wavelength scanning. The transmitted light from the microcavity is directed into a 90/10 fiber coupler. The 10% output port is recorded by an optical spectrum analyzer (OSA, AQ6370D, Yokogawa), whereas the 90% port is collected by a low-noise photodetector (PD, PDB450C, Thorlabs) and analyzed by an oscilloscope (OSC, DLM3034, Yokogawa). To photothermally tune the microcavity, several pump lasers with wavelengths of 780, 850, 940, 980, and 1064 nm are, individually, axially injected into the microcavity through the fiber stem to act as heating sources and thereby trigger the photothermal effect. An optical power meter (OPM, PM100D, Thorlabs) is used to record the pump power exerting on the microcavity. The evanescent coupling between the microcavity and the tapered fiber is controlled by adjusting the distance between them, which can be accomplished by using a three-dimensional motorized translation stage (NanoMax 300, Thorlabs). The adjusting process is monitored in real time under an imaging system consisting of a CCD camera and a 10× objective (NA = 0.28). A dark-field micrograph illustrating the microcavity coupled to the tapered fiber is given in the top left inset of Fig. 1(b) in the main text. The microcavity-based coupled device is placed inside a home-built chamber to minimize the interference from air flow and contaminants.

SUPPLEMENTARY MATERIAL

See the supplementary material for additional microcavity fabrication and experimental setup, numerical simulation of optical resonance in the microcavity, Q-factor characterization, transmission spectra, performance comparison of photothermal tunable microcavities, detection limit of the pump power, principle of the decoupling strategy for parallel measurement, and calculation of RMSE.

ACKNOWLEDGMENTS

This work was supported by the National Natural Science Foundation of China (NSFC) (Grant Nos. 11935006, 11774086, 92365107, 12247105, 12175060, 12205256, 11935006, 12405029, 12304474, and 12304407); The National Key R&D Program of China (Grant Nos. 2019YFA0308700 and 2019YFA0308704); The Program for Innovative Talents and Teams in Jiangsu (Grant No. JSSCTD202138); State Key Laboratory of Advanced Optical Communication Systems and Networks, China (Grant No. 2024GZKF14); Joint Fund of Henan Province Science and Technology R&D Program (Grant No. 225200810071); The Science and Technology Major Project of Henan Province (Grant No. 231100220800); HNQSTIT project (Grant No. 2022112); The Henan Science and Technology Major Project of the Department of Science and Technology of Henan Province (Grant No. 241100210400); Doctoral Research Foundation (Grant No. 2022BSJJZK18); and The Natural Science Foundation of Henan Province (Grant No. 252300421221).

AUTHOR DECLARATIONS

Conflict of Interest

The authors have no conflicts to disclose.

Author Contributions

Yan Wang: Conceptualization (equal); Formal analysis (equal); Investigation (equal); Methodology (equal); Writing – original draft (equal). **Yu-Hao Hu:** Data curation (equal); Formal analysis (equal); Investigation (equal); Methodology (equal); Writing – original draft (equal). **Jin-Lei Wu:** Formal analysis (equal); Investigation (equal); Visualization (equal). **Jian Tang:** Formal analysis (equal); Software (equal). **Ya-Feng Jiao:** Formal analysis (equal); Software (equal). **Ya-Chuan Liang:** Formal analysis (equal); Visualization (equal). **Haiyan Wang:** Supervision (supporting). **Liying Jiang:** Supervision (supporting). **Le-Man Kuang:** Supervision (equal); Validation (equal). **Keyu Xia:** Funding acquisition (equal); Supervision (equal); Writing – review & editing (equal). **Lei Shi:** Funding acquisition (equal); Supervision (equal); Writing – review & editing (equal). **Hui Jing:** Funding acquisition (equal); Supervision (equal); Writing – review & editing (equal).

DATA AVAILABILITY

The data that support the findings of this study are available from the corresponding authors upon reasonable request.

REFERENCES

[1]J. Cho, X. Chen, G. Raybon, D. Che, E. Burrows, S. Olsson, and R. Tkach, "Shaping lightwaves in time and frequency for optical fiber communication," Nat. Commun. **13**, 785 (2022).
[2]M. Jin, S.-J. Tang, J.-H. Chen, X.-C. Yu, H. Shu, Y. Tao, A. K. Chen, Q. Gong, X. Wang, and Y.-F. Xiao, "1/f-noise-free optical sensing with an integrated heterodyne interferometer," Nat. Commun. **12**, 1973 (2021).
[3]Y. Zhang, S. Zhu, J. Hu, and M. Gu, "Femtosecond laser direct nanolithography of perovskite hydration for temporally programmable holograms," Nat. Commun. **15**, 6661 (2024).
[4]J. Franke, S. R. Muleady, R. Kaubruegger, F. Kranzl, R. Blatt, A. M. Rey, M. K. Joshi, and C. F. Roos, "Quantum-enhanced sensing on optical transitions through finite-range interactions," Nature **621**, 740 (2023).
[5]G. Huang, A. Beccari, N. J. Engelsen, and T. J. Kippenberg, "Room-temperature quantum optomechanics using an ultralow noise cavity," Nature **626**, 512–516 (2024).
[6]L. Hartung, M. Seubert, S. Welte, E. Distante, and G. Rempe, "A quantum-network register assembled with optical tweezers in an optical cavity," Science **385**, 179–183 (2024).

[7]N. K. Metzger, R. Spesyvtsev, G. D. Bruce, B. Miller, G. T. Maker, G. Malcolm, M. Mazilu, and K. Dholakia, "Harnessing speckle for a sub-femtometre resolved broadband wavemeter and laser stabilization," Nat. Commun. **8**, 15610 (2017).
[8]H. Xu, Y. Qin, G. Hu, and H. K. Tsang, "Breaking the resolution-bandwidth limit of chip-scale spectrometry by harnessing a dispersion-engineered photonic molecule," Light. Sci. Appl. **12**, 64 (2023).
[9]E. Edrei, N. Cohen, E. Gerstel, S. Gamzu-Letova, N. Mazurski, and U. Levy, "Chip-scale atomic wavemeter enabled by machine learning," Sci. Adv. **8**, eabn3391 (2022).
[10]R. Niu, M. Li, S. Wan, Y. R. Sun, S.-M. Hu, C.-L. Zou, G.-C. Guo, and C.-H. Dong, "kHz-precision wavemeter based on reconfigurable microsoliton," Nat. Commun. **14**, 169 (2023).
[11]I. Coddington, N. Newbury, and W. Swann, "Dual-comb spectroscopy," Optica **3**, 414–426 (2016).
[12]B. Bernhardt, A. Ozawa, P. Jacquet, M. Jacquey, Y. Kobayashi, T. Udem, R. Holzwarth, G. Guelachvili, T. W. Hänsch, and N. Picqué, "Cavity-enhanced dual-comb," Spectrosc. Nat. Photonics **4**, 55–57 (2010).
[13]B. Redding, S. F. Liew, R. Sarma, and H. Cao, "Compact spectrometer based on a disordered photonic chip," Nat. Photonics **7**, 746–751 (2013).
[14]M. Faraji-Dana, E. Arbabi, A. Arbabi, S. M. Kamali, H. Kwon, and A. Faraon, "Compact folded metasurface spectrometer," Nat. Commun. **9**, 4196 (2018).
[15]A. Li and Y. Fainman, "On-chip spectrometers using stratified waveguide filters," Nat. Commun. **12**, 2704 (2021).
[16]C. Yao, K. Xu, W. Zhang, M. Chen, Q. Cheng, and R. Penty, "Integrated reconstructive spectrometer with programmable photonic circuits," Nat. Commun. **14**, 6376 (2023).
[17]F. Monifi, J. Zhang, ŞK. Özdemir, B. Peng, Y.-X. Liu, F. Bo, F. Nori, and L. Yang, "Optomechanically induced stochastic resonance and chaos transfer between optical fields," Nat. Photonics **10**, 399–405 (2016).
[18]Z. Shen, Y.-L. Zhang, Y. Chen, C.-L. Zou, Y.-F. Xiao, X.-B. Zou, F.-W. Sun, G.-C. Guo, and C.-H. Dong, "Experimental realization of optomechanically induced non-reciprocity," Nat. Photonics **10**, 657–661 (2016).
[19]M. Asano, H. Yamaguchi, and H. Okamoto, "Free-access optomechanical liquid probes using a twin-microbottle resonator," Sci. Adv. **8**, eabq2502 (2022).
[20]T. X. Lu, Y. Wang, K. Xia, X. Xiao, L. M. Kuang, and H. Jing, "Quantum squeezing induced nonreciprocal phonon laser," Sci. China-Phys. Mech. Astron **67**, 260312 (2024).
[21]A. Li, H. Wei, M. Cotrufo, W. Chen, S. Mann, X. Ni, B. Xu, J. Chen, J. Wang, S. Fan, C.-W. Qiu, A. Alù, and L. Chen, "Exceptional points and non-Hermitian photonics at the nanoscale," Nat. Nanotechnol. **18**, 706–720 (2023).
[22]B. Chen, Y. Zhou, Y. Liu, C. Ye, Q. Cao, P. Huang, C. Kim, Y. Zheng, L. K. Oxenløwe, K. Yvind, J. Li, J. Li, Y. Zhang, C. Dong, S. Fu, Q. Zhan, X. Wang, M. Pu, and J. Liu, "Integrated optical vortex microcomb," Nat. Photonics **18**, 625–631 (2024).
[23]W. Mao, Y. Li, X. Jiang, Z. Liu, and L. Yang, "A whispering-gallery scanning microprobe for Raman spectroscopy and imaging," Light: Sci. Appl. **12**, 247 (2023).
[24]B. B. Li, W. R. Clements, X. C. Yu, K. Shi, Q. Gong, and Y. F. Xiao, "Single nanoparticle detection using split-mode microcavity Raman lasers," Proc. Natl. Acad. Sci. U. S. A. **111**, 14657–14662 (2014).
[25]P. J. Zhang, Q. X. Ji, Q. T. Cao, H. Wang, W. Liu, Q. Gong, and Y. F. Xiao, "Single-mode characteristic of a supermode microcavity Raman laser," Proc. Natl. Acad. Sci. U. S. A. **118**, e2101605118 (2021).
[26]R. Duan, Z. Zhang, L. Xiao, X. Zhao, Y. T. Thung, L. Ding, Z. Liu, J. Yang, V. D. Ta, and H. Sun, "Ultralow-threshold and high-quality whispering-gallery-mode lasing from colloidal core/hybrid-shell quantum wells," Adv. Mater. **34**, 2108884 (2022).
[27]C. Gong, X. Yang, S.-J. Tang, Y.-C. Chen, Q.-Q. Zhang, Y. Wang, Y.-L. Liu, G.-D. Peng, X. Fan, Y.-F. Xiao, Y.-J. Rao, and Y. Gong, "Submonolayer biolasers for ultrasensitive biomarker detection," Light: Sci. Appl. **12**, 292 (2023).
[28]J. Zhu, ŞK. Özdemir, Y. F. Xiao, L. Li, L. He, D. R. Chen, and L. Yang, "On-chip single nanoparticle detection and sizing by mode splitting in an ultrahigh-Q microresonator," Nat. Photonics **4**, 46–49 (2010).
[29]L. He, ŞK. Özdemir, J. Zhu, W. Kim, and L. Yang, "Detecting single viruses and nanoparticles using whispering gallery microlasers," Nat. Nanotechnol. **6**, 428–432 (2011).
[30]X. C. Yu, S. J. Tang, W. Liu, Y. Xu, Q. Gong, Y. L. Chen, and Y. F. Xiao, "Single-molecule optofluidic microsensor with interface whispering gallery modes," Proc. Natl. Acad. Sci. U. S. A. **119**, e2108678119 (2022).
[31]S.-J. Tang, M. Zhang, J. Sun, J.-W. Meng, X. Xiong, Q. Gong, D. Jin, Q.-F. Yang, and Y.-F. Xiao, "Single-particle photoacoustic vibrational spectroscopy using optical microresonators," Nat. Photonics **17**, 951–956 (2023).
[32]K. J. Vahala, "Optical microcavities," Nature **424**, 839–846 (2003).
[33]X. Jiang, A. J. Qavi, S. H. Huang, and L. Yang, "Whispering-gallery sensors," Matter **3**, 371–392 (2020).
[34]M. R. Foreman, J. D. Swaim, and F. Vollmer, "Whispering gallery mode sensors," Adv. Opt. Photonics **7**, 168–240 (2015).
[35]L. Shao, X. F. Jiang, X. C. Yu, B. B. Li, W. R. Clements, F. Vollmer, W. Wang, Y. F. Xiao, and Q. Gong, "Detection of single nanoparticles and lentiviruses using microcavity resonance broadening," Adv. Mater. **25**, 5616–5620 (2013).
[36]K. D. Heylman, N. Thakkar, E. H. Horak, S. C. Quillin, C. Cherqui, K. A. Knapper, D. J. Masiello, and R. H. Goldsmith, "Optical microresonators as single-particle absorption spectrometers," Nat. Photonics **10**, 788–795 (2016).
[37]Z.-G. Hu, Y.-M. Gao, J.-F. Liu, H. Yang, M. Wang, Y.-C. Lei, X. Zhou, J.-C. Li, X. Cao, J. Liang, C.-Q. Hu, Z. Li, Y.-C. Lau, J.-W. Cai, and B.-B. Li, "Picotesla-sensitivity microcavity optomechanical magnetometry," Light: Sci. Appl. **13**, 279 (2024).
[38]M. Humar, M. Ravnik, S. Pajk, and I. Muševič, "Electrically tunable liquid crystal optical microresonators," Nat. Photonics **3**, 595–600 (2009).
[39]Y. Liu, L. Shi, X. Xu, P. Zhao, Z. Wang, S. Pu, and X. Zhang, "All-optical tuning of a magnetic-fluid-filled optofluidic ring resonator," Lab Chip **14**, 3004–3010 (2014).
[40]P. Zhao, L. Shi, Y. Liu, Z. Wang, S. Pu, and X. Zhang, "Iron-oxide nanoparticles embedded silica microsphere resonator exhibiting broadband all-optical wavelength tunability," Opt. Lett. **39**, 3845–3848 (2014).
[41]R. Duan, J. Sun, Y. Zhang, H. Li, Y. Li, and Z. Liu, "A non-volatile quasi-continuous all-optical fiber programmable platform based on GST-coated microspheres," ACS Photonics **9**, 1180–1187 (2022).
[42]D. Q. Yang, J. H. Chen, Q. T. Cao, B. Duan, H. J. Chen, X. C. Yu, and Y. F. Xiao, "Operando monitoring transition dynamics of responsive polymer using optofluidic microcavities," Light: Sci. Appl. **10**, 128 (2021).
[43]Y. Wu, B. Duan, J. Song, H. Tian, J. H. Chen, D. Yang, and S. Huang, "Simultaneous temperature and pressure sensing based on a single optical resonator," Opt. Express **31**, 18851–18861 (2023).
[44]S. Zhu, L. Shi, S. Yuan, X. Xu, and X. Zhang, "All-optical control of ultrahigh-Q silica microcavities with iron oxide nanoparticles," Opt. Lett. **42**, 5133–5136 (2017).
[45]S. Zhu, L. Shi, B. Xiao, X. Zhang, and X. Fan, "All-optical tunable microlaser based on an ultrahigh-Q erbium-doped hybrid microbottle cavity," ACS Photonics **5**, 3794–3800 (2018).
[46]S. Zhu, B. Xiao, B. Jiang, L. Shi, and X. Zhang, "Tunable Brillouin and Raman microlasers using hybrid microbottle resonators," Nanophotonics **8**, 931–940 (2019).
[47]W. Lin, H. Zhang, B. Liu, B. Song, Y. Li, C. Yang, and Y. Liu, "Laser-tuned whispering gallery modes in a solid-core microstructured optical fibre integrated with magnetic fluids," Sci. Rep. **5**, 17791 (2015).
[48]Y. Chen, X. Zhang, Q. Zhang, Z. Wang, J. Fei, Y. Yang, Y. Wang, Y. Yu, Y. Dong, Y. Huang, and T. Wang, "All-optical tuning of microbottle resonator assisted by a movable probe with magnetic nanoparticles," IEEE Sens. J. **23**, 2153–2158 (2023).
[49]Y. Huang, S. Liao, B. Tu, Q. Xu, Z. Zeng, and C. Xu, "All-optical tuning of the frequency of Yb3+/Er3+ co-doped microsphere WGM laser pumped by 1 μm ASE light source," Opt. Laser Technol. **169**, 109907 (2024).
[50]X. Hao, S. Zhao, J. Gao, and L. Suo, "All-optical tunable whispering gallery mode lasing in a PMMA-coated microcavity embedded with a high-efficiency nanoheater," Opt. Laser Technol. **164**, 109527 (2023).
[51]H. Wang, M. Liao, H. Xiao, Z. Zhang, J. Yang, J. Yang, and Y. Tian, "All-optical tunable whispering gallery modes in a polymer bottle micro-resonator," IEEE Photonics Technol. Lett. **33**, 97–100 (2021).
[52]B. Niu, X. Shi, K. Ge, J. Ruan, Z. Xu, S. Zhang, D. Guo, and T. Zhai, "An all-optical tunable polymer WGM laser pumped by a laser diode," Nanoscale Adv. **4**, 2153–2158 (2022).
[53]A. K. Nowak, S. L. Portalupi, V. Giesz, O. Gazzano, C. Dal Savio, P.-F. Braun, K. Karrai, C. Arnold, C. Lanco, I. Sagnes, A. Lemaître, and P. Senellart, "Deterministic and electrically tunable bright single-photon source," Nat. Commun. **5**, 3240 (2014).

[54]Y. K. Thomas, D. A. Bracht, F. Kappe, P. C. A. Hagen, C. Schimpf, J. C. Loredo, V. Remesh, S. F. Covre da Silva, L. M. Hansen, R. Schwarz, P. Walther, A. Rastelli, V. M. Axt, T. Heindel, D. E. Reiter, and G. Weihs, "Controlling the photon number coherence of solid-state quantum light sources for quantum cryptography," npj Quantum Inf. **10**, 17 (2024).
[55]K. Sugioka and Y. Cheng, "Ultrafast lasers—Reliable tools for advanced materials processing," Light. Sci. Appl. **3**, e149 (2014).
[56]C. Y. Tan, C. Wen, and H. Q. Ang, "Influence of laser parameters on the microstructures and surface properties in laser surface modification of biomedical magnesium alloys," J. Magnes. Alloys **12**, 500–512 (2024).
[57]O. Gaathon, J. Culic-Viskota, M. Mihnev, I. Teraoka, and S. Arnold, "Enhancing sensitivity of a whispering gallery mode biosensor by subwavelength confinement," Appl. Phys. Lett **89**, 223901 (2006).
[58]C. Lozano-Pedraza, E. Plaza-Mayoral, A. Serrano, D. Felder-Flesch, G. Salas, A. Espinosa, B. Sot, C. Blanco-Andujar, G. Cotin, S. Begin-Colin, and F. J. Teran, "Assessing the parameters modulating optical losses of iron oxide nanoparticles under near infrared irradiation," Nanoscale Adv. **3**, 6490–6502 (2021).
[59]Y. Z. Yan, C. L. Zou, S. B. Yan, F. W. Sun, Z. Ji, J. Liu, Y. G. Zhang, L. Wang, C. Y. Xue, W. D. Zhang, Z. F. Han, and J. J. Xiong, "Packaged silica microsphere-taper coupling system for robust thermal sensing application," Opt. Express **19**, 5753–5759 (2011).
[60]Y. Z. Yan, C. L. Zou, S. B. Yan, F. W. Sun, J. Liu, C. Y. Xue, Y. G. Zhang, L. Wang, W. D. Zhang, and J. J. Xiong, "Robust spot-packaged microsphere-taper coupling structure for in-line optical sensors," IEEE Photonics Technol. Lett. **23**, 1736–1738 (2011).
[61]Y. Dong, K. Wang, and X. Jin, "Packaged microsphere-taper coupling system with a high Q factor," Appl. Opt. **54**, 277–284 (2015).
[62]H. Wang, Y.-M. He, T. H. Chung, H. Hu, Y. Yu, S. Chen, X. Ding, M.-C. Chen, J. Qin, X. Yang, R.-Z. Liu, Z.-C. Duan, J.-P. Li, S. Gerhardt, K. Winkler, J. Jurkat, L.-J. Wang, N. Gregersen, Y.-H. Huo, Q. Dai, S. Yu, S. Höfling, C.-Y. Lu, and J.-W. Pan, "Towards optimal single-photon sources from polarized microcavities," Nat. Photonics **13**, 770–775 (2019).
[63]S. Gyger, J. Zichi, L. Schweickert, A. W. Elshaari, S. Steinhauer, S. F. Covre da Silva, A. Rastelli, V. Zwiller, K. D. Jöns, and C. Errando-Herranz, "Reconfigurable photonics with on-chip single-photon detectors," Nat. Commun. **12**, 1408 (2021).
[64]R. R. Gattass and E. Mazur, "Femtosecond laser micromachining in transparent materials," Nat. Photonics **2**, 219–225 (2008).
[65]H. S. Jung, P. Verwilst, A. Sharma, J. Shin, J. L. Sessler, and J. S. Kim, "Organic molecule-based photothermal agents: An expanding photothermal therapy universe," Chem. Soc. Rev. **47**, 2280–2297 (2018).
[66]Y. Liu, P. Bhattarai, Z. Dai, and X. Chen, "Photothermal therapy and photoacoustic imaging via nanotheranostics in fighting cancer," Chem. Soc. Rev. **48**, 2053–2108 (2019).